# Section Chern number for a 3D photonic crystal and the bulk-edge correspondence

Shuhei Oono,[1,*] Toshikaze Kariyado,[1,2] and Yasuhiro Hatsugai[1]

[1] *Graduate School of Pure and Applied Science, University of Tsukuba, Tsukuba 305-8577, Japan*
[2] *International Center for Materials Nanoarchitectonics, National Institute for Materials Science, Tsukuba 305-0047, Japan*

We have characterized the robust propagation modes of electromagnetic waves in helical structures by the section Chern number that is defined for a two-dimensional (2D) section of the three-dimensional (3D) Brillouin zone. The Weyl point in the photonic bands is associated with a discontinuous jump of the section Chern number. A spatially localized Gaussian basis set is used to calculate the section Chern numbers where we have implemented the divergence-free condition on each basis function in 3D. The validity of the bulk-edge correspondence in a 3D photonic crystal is discussed in relation to the broken inversion symmetry.

arXiv:1607.04714v2 [physics.optics] 14 Sep 2016

## I. INTRODUCTION

Photonic crystals[1–3] are systems with a spatially periodic structure of refractive medium. Electromagnetic (EM) fields in a photonic crystal are given by the Bloch states where frequency dispersion may have an energy gap as the electronic band dispersion of solids. This gives us an opportunity to simulate microscopic quantum states of electrons by the macroscopic EM waves governed by the classical Maxwell equations. Especially, simulating topologically nontrivial phases in quantum solids has been an extensively studied topic these days. A prototypical topological phase of matter is an integer quantum Hall state[4], where its topological nature is encoded in a topological invariant, the Chern number, calculated using the Bloch wave functions[5]. A physical consequence of the topological nature is quantization of the Hall conductance, since it is proportional to the Chern number. On the other hand, the quantization is also explained in terms of the chiral edge states[6,7]. Generally, there is an intimate relation between bulk topology and edge states, as known as the bulk-edge correspondence[8]. So, we can access topological properties of the bulk via edge states, or inversely, we can know about the edge/surface states by the bulk information alone.

The idea of the bulk-edge correspondence is especially important in photonic systems[9–21], since there is no "Hall conductance" in photonic systems, while edge states are always physical observable. Since we have the Bloch states and the Brillouin zone in periodic photonic systems, the Chern number is well-defined as in electronic systems. Then, comparing the bulk Chern number and the edge states is a natural strategy to attack topological issues in photonic systems. In fact, quantum Hall state analogs in 2D photonic crystals have been discussed focusing on the edge states. Note that in such studies, the time reversal symmetry (TRS) breaking is mandatory to realize a quantum Hall analog.

In this paper, a Gaussian type localized basis set based method is introduced for numerical evaluation of the Bloch states of the EM waves. With the localized basis set, momentum, which defines the Brillouin zone, is treated as a twisted boundary condition $e^{i\phi_\alpha}$, $\alpha = x, y$, and then, the basis functions naturally and strictly becomes periodic in momentum $\phi_\alpha$. Since we will explain later, this feature is advantageous in the Chern number calculation, and this is the reason for our choice of the localized basis set. The Gaussian expansion is not the only choice for the localized basis set, i.e., for instance, the finite element method[22–26] gives an alternative. However, the Gaussian basis element is convenient when derivatives of the basis functions are required, obviously due to its Gaussian nature. Such a situation really arises in 3D crystals where the decomposition of the EM field into TE or TM modes is impossible. We demonstrate the merit of the Gaussian expansion through the calculation of the "section" Chern numbre[27–30] of the 3D photonic crystals.

As we explained, the introduced method is applied to 3D photonic crystals. First of all, note that it is possible to define and use the Chern number to characterize the given system even in 3D cases as follows. That is, let us fix one of the three components of the momentum, say $k_3$, and define the Chern number $C(k_3)$ using $(k_1, k_2)$ as a periodic parameter space. Since this parameter space is a 2D section of the 3D Brillouin zone, we call $C(k_3)$ the section Chern number. This section Chern number is well defined only when the band gap is always finite on the constant $k_3$ plane (section). Different from the usual Chern number in 2D systems, the section Chern number can be finite even in systems having TRS. This feature enables us to realize a topologically nontrivial state in photonic crystals without magneto-optical media. Specifically, $C(k_3)$ can take a nonzero value when the TRS *or* the spatial inversion symmetry (SIS) is broken.

Since the section Chern number $C(k_i)$ is a topological invariant, it can change only when the band gap vanishes at a certain point on the constant $k_i$ plane. Generally, this gap closing point is a Weyl point in the band structure, having a linear dispersion around it. Intriguing topological properties are expected in the system with the Weyl points[31–34]. Also, it has been already shown that the Weyl points emerge in the double gyroid photonic crystal when TRS or SIS is broken[18,20].

In this paper, we consider a photonic crystal of a sim-

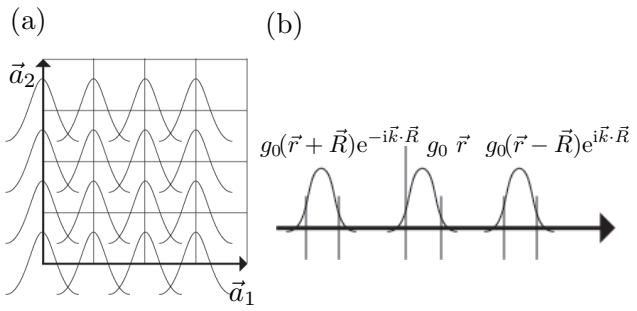


FIG. 1. (a) Gaussian (spatially localized) basis elements are put on the grid that divides unit cell uniformly in the directions of $\boldsymbol{a}_1$ and $\boldsymbol{a}_2$. (b) Each basis element is set on each unit cell with the factor $\mathrm{e}^{\mathrm{i}\boldsymbol{k}\cdot\boldsymbol{R}}$.

ple structure with Weyl points to discuss the topological nature. In this paper, we limit ourselves to the cases with TRS but without SIS. The considered system is anisotropic and the Weyl points are clearly resolved only in a constant $k_z$ plane in the Brillouin zone. We also discuss the edge states associated with the nonzero section Chern number, which can be realized by making a wave packet.

This paper is organized as follows. In Sec. II, we introduce the Gaussian expansion method for the photonic crystals, and explain the importance of the localized basis set for the calculation of the Chern number. Section III is devoted to demonstrate the validity and the usefulness of the introduced method by applying the method to simple models. In Sec. IV, a specific photonic crystal having the Weyl points in its photonic band structure is proposed, and the section Chern number for that model is evaluated. The relation between the section Chern number and the edge modes is also discussed. Summary and discussion are given in Sec. V.

## II. METHODS

The Maxwell equations for the normal modes introduced as $\boldsymbol{E}(\boldsymbol{r},t)=\mathrm{e}^{-\mathrm{i}\omega t}\boldsymbol{E}(\boldsymbol{r})$ and $\boldsymbol{H}(\boldsymbol{r},t)=\mathrm{e}^{-\mathrm{i}\omega t}\boldsymbol{H}(\boldsymbol{r})$ are written as

$$\begin{aligned}\nabla\times\boldsymbol{E}(\boldsymbol{r})=\mathrm{i}\omega\boldsymbol{B}(\boldsymbol{r}),\quad \nabla\times\boldsymbol{H}(\boldsymbol{r})=-\mathrm{i}\omega\boldsymbol{D}(\boldsymbol{r}),\\ \nabla\cdot\boldsymbol{D}(\boldsymbol{r})=0,\qquad\quad \nabla\cdot\boldsymbol{B}(\boldsymbol{r})=0.\end{aligned}\tag{1}$$

Here, we assume that the permittivity and the permeability are linear and lossless, i.e., we assume

$$\boldsymbol{D}(\boldsymbol{r})=\varepsilon_0\hat{\varepsilon}(\boldsymbol{r})\,\boldsymbol{E}(\boldsymbol{r})\,,\ \boldsymbol{B}(\boldsymbol{r})=\mu_0\hat{\mu}(\boldsymbol{r})\,\boldsymbol{E}(\boldsymbol{r})\,,\tag{2}$$

where $\hat{\varepsilon}(\boldsymbol{r})$ and $\hat{\mu}(\boldsymbol{r})$ are $3\times3$ tensors satisfying the Hermitian conditions $\hat{\varepsilon}^\dagger=\hat{\varepsilon}$ and $\hat{\mu}^\dagger=\hat{\mu}$. With this assumption, the Maxwell equations are rewritten into Hermitian eigenequation forms as

$$\nabla\times\hat{\varepsilon}^{-1}(\boldsymbol{r})\,\nabla\times\boldsymbol{H}(\boldsymbol{r})=\left(\frac{\omega}{c}\right)^2\hat{\mu}(\boldsymbol{r})\,\boldsymbol{H}(\boldsymbol{r})\,,\tag{3}$$

$$\nabla\times\hat{\mu}^{-1}(\boldsymbol{r})\nabla\times\boldsymbol{E}(\boldsymbol{r})=\left(\frac{\omega}{c}\right)^2\hat{\varepsilon}(\boldsymbol{r})\,\boldsymbol{E}(\boldsymbol{r})\,.\tag{4}$$

We only have to solve the either of these eigenequations with respect to $\boldsymbol{E}$ or $\boldsymbol{H}$. In a spatially periodic system, all the eigenstates are represented as Bloch states.

Roughly speaking, there are two ways to expand a Bloch state. The first way is to use a basis set localized in wave space like plane waves[35–39], and the second way is to use a basis set localized in real space. For the plane wave type basis sets , a Bloch state is usually represented as

$$\psi_k(\boldsymbol{r})=\sum_G f_G\mathrm{e}^{\mathrm{i}(\boldsymbol{G}+\boldsymbol{k})\cdot\boldsymbol{r}},\tag{5}$$

with $\boldsymbol{G}$ denoting reciprocal lattice vectors. In this form, each basis element is not periodic for a parameter change $\boldsymbol{k}\to\boldsymbol{k}+\boldsymbol{G}$, since $\mathrm{e}^{\mathrm{i}\boldsymbol{k}\cdot\boldsymbol{r}}$ and $\mathrm{e}^{\mathrm{i}(\boldsymbol{G}+\boldsymbol{k})\cdot\boldsymbol{r}}$ are not identical.

On the other hand, for spatially localized basis sets, the matrix eigenequation can be naturally made into periodic in parameter $k$. A Bloch state is represented by localized basis set as

$$\psi_k(\boldsymbol{r})=\frac{1}{\sqrt{N}}\sum_m\mathrm{e}^{\mathrm{i}\boldsymbol{k}\cdot\boldsymbol{R}_m}w_m(\boldsymbol{r})\,,\tag{6}$$

with $\boldsymbol{R}_m$ and $N$ representing a lattice vector in real space and the number of unit cells of the system under consideration respectively, and $w_m(\boldsymbol{r})=w_0(\boldsymbol{r}-\boldsymbol{R}_m)$. In this form, a parameter $k$ only appears as $\boldsymbol{e}^{\mathrm{i}\boldsymbol{k}\cdot\boldsymbol{R}_m}$ and is introduced in the eigenequation as a boundary condition. This periodicity is crucial in the numerical evaluation of the Chern number[40].

Representative localized functions are the maximally localized Wannier functions[41–44], however, it is known that the so-called *composite bands*, which compose the maximally localized Wannier functions, must be distinguished from the bands below and above by gaps with vanishing Chern number[45,46]. However, photonic bands are generally tangling in higher frequencies and it is not common for photonic band structures to have an isolated set of bands enclosed by gaps.

Then, we use a Gaussian basis set as a typical localized basis set in the following. Explicitly, the Gaussian basis element is written as

$$\boldsymbol{g}^\lambda_{i,k}(\boldsymbol{r})=\frac{1}{\sqrt{N}}\sum_{m,\lambda}\mathrm{e}^{\mathrm{i}\boldsymbol{k}\cdot\boldsymbol{R}_m}\boldsymbol{f}^\lambda(\boldsymbol{r}_{im})\,\mathrm{e}^{-r_{im}^2/\alpha^2},\tag{7}$$

with

$$\boldsymbol{f}^\lambda(\boldsymbol{r}_{im})=\begin{pmatrix}f_x^\lambda(x_{im},y_{im},z_{im})\\ f_y^\lambda(x_{im},y_{im},z_{im})\\ f_z^\lambda(x_{im},y_{im},z_{im})\end{pmatrix}.\tag{8}$$

Here, suffices $i$ and $\lambda$ specify the grid position within the unit cell and the polarization degrees of freedom respectively, and $\boldsymbol{r}_{im} = \boldsymbol{r} - (\boldsymbol{R}_m + \boldsymbol{r}_i)$. The $f_i^\lambda(x,y,z)$ is a polynomial of $(x,y,z)$. Using this basis set for the eigenfunction expansion in Eq. (3), we obtain a matrix eigenequation

$$\sum_{j,\lambda'} \Theta_{i\lambda,j\lambda'}(\boldsymbol{k})\, c_j^{\lambda'} = \left(\frac{\omega}{c}\right)^2 \sum_{j,\lambda'} O_{i\lambda,j\lambda'}(\boldsymbol{k})\, c_j^{\lambda'}. \quad (9)$$

Here, $\Theta_{i\lambda,j\lambda'}(\boldsymbol{k})$ is the matrix element of the operator in the left hand side of Eq. (3), i.e., $\hat{\Theta} = \nabla \times \hat{\varepsilon}^{-1}(\boldsymbol{r})\, \nabla\times$, which is explicitly written as

$$\begin{aligned}\Theta_{i\lambda,j\lambda'}(\boldsymbol{k}) &= \left\langle \boldsymbol{g}_{ik}^{\lambda} \right| \nabla \times \hat{\varepsilon}^{-1}(\boldsymbol{r})\, \nabla \times \left| \boldsymbol{g}_{jk}^{\lambda'} \right\rangle \\ &= \sum_m \mathrm{e}^{-\mathrm{i}\boldsymbol{k}\cdot\boldsymbol{R}_m} \int \mathrm{d}^3 r \left(\nabla \times \boldsymbol{f}^\lambda(\boldsymbol{r}_{im})\, \mathrm{e}^{-r_{im}^2/\alpha^2}\right)^* \\ &\quad \cdot \hat{\varepsilon}^{-1}(\boldsymbol{r}) \left(\nabla \times \boldsymbol{f}^\lambda(\boldsymbol{r}_{j0})\, \mathrm{e}^{-r_{j0}^2/\alpha^2}\right). \quad (10)\end{aligned}$$

Here we used the Hermiticity of the rotation, $\int \mathrm{d}^3 r\, \boldsymbol{g}^*(\boldsymbol{r}) \cdot \{\nabla \times \boldsymbol{f}(\boldsymbol{r})\} = \int \mathrm{d}^3 r\, \boldsymbol{f}(\boldsymbol{r}) \cdot \{\nabla \times \boldsymbol{g}(\boldsymbol{r})\}^*$ under the boundary condition, $\lim_{r\to\infty} \boldsymbol{g}_{i,k}^{\lambda}(\boldsymbol{r}) = 0$. On the other hand, $O_{i\lambda,j\lambda'}(\boldsymbol{k})$ is the overlap, which is obtained as,

$$\begin{aligned}O_{i\lambda,j\lambda'}(\boldsymbol{k}) &= \left\langle \boldsymbol{g}_{ik}^{\lambda} \right| \hat{\mu}(\boldsymbol{r}) \left| \boldsymbol{g}_{jk}^{\lambda'} \right\rangle \\ &= \sum_m \mathrm{e}^{-\mathrm{i}\boldsymbol{k}\cdot\boldsymbol{R}_m} \int \mathrm{d}^3 r \left(\boldsymbol{f}^\lambda(\boldsymbol{r}_{im})\, \mathrm{e}^{-r_{im}^2/\alpha^2}\right)^* \\ &\quad \cdot \hat{\mu}(\boldsymbol{r}) \left(\boldsymbol{f}^{\lambda'}(\boldsymbol{r}_{j0})\, \mathrm{e}^{-r_{j0}^2/\alpha^2}\right). \quad (11)\end{aligned}$$

The integration is performed over the infinite spatial region. In many cases, a photonic crystal is constituted by repetition of structures having different permittivity or permeability from the uniform media. Then, it is convenient to separate the inverse of permittivity $\hat{\varepsilon}^{-1}(\boldsymbol{r})$ as

$$\hat{\varepsilon}^{-1}(\boldsymbol{r}) = \hat{\varepsilon}_c^{-1} + \left(\hat{\varepsilon}^{-1}(\boldsymbol{r}) - \hat{\varepsilon}_c^{-1}\right). \quad (12)$$

The first term of the right hand side is constant corresponding to the uniform background media. The second term is nonzero only in the region where the structures exist. For the constant term, the integrals of the matrix elements are the standard Gaussian integral, which can be analytically evaluated. For the second term, the numerical integration is easy since the integrand is finite only in the limited region. The same argument also applies to the inverse of the permeability $\hat{\mu}^{-1}(\boldsymbol{r})$. For a uniform system all the matrix elements are given without numerical integration.

### A. Gaussian basis set (2D case)

First, we consider the 2D case. Here, 2D means that $\hat{\varepsilon}(\boldsymbol{r})$ and $\hat{\mu}(\boldsymbol{r})$ have no dependence on $z$. In such a system, a mirror plane perpendicular to the $z$ axis exists and the solutions of Eqs. (3) and (4) are separated into TE modes ($H_z$ polarization) or TM modes ($E_z$ polarization). As a result, we only have to consider the $z$ component of either field $\boldsymbol{H}$ or $\boldsymbol{E}$, which indicates that the equation to be solved becomes a scalar equation.

For the scalar eigenequation, we use a basis element

$$g_{ik}(\boldsymbol{r}) = \frac{1}{\sqrt{N}} \sum_m \mathrm{e}^{\mathrm{i}\boldsymbol{k}\cdot\boldsymbol{R}_m} \mathrm{e}^{-r_{im}^2/\alpha^2}. \quad (13)$$

Each basis function is cylindrically symmetric and there are finite overlaps between the basis functions. Then, these basis elements are put on the grid dividing the unit cell regularly (Fig.1). Later, we will see that the simple configuration of the basis elements gives sufficient accuracy for our purpose, and there arises no need for further attention on the distribution of the grids, which is often important in the standard finite element methods.

For this basis set, the integral of the overlap $O_{ij}(\boldsymbol{k})$ for the constant term (when $\hat{\mu}_c = \hat{1}$) is obtained as

$$O_{ij}^{\mathrm{empty}}(\boldsymbol{k}) = \sum_m \frac{\pi\alpha^2}{2} \mathrm{e}^{-\mathrm{i}\boldsymbol{k}\cdot\boldsymbol{R}_m} \mathrm{e}^{-\frac{{r'_m}^2}{2\alpha^2}}, \quad (14)$$

where $\boldsymbol{r}'_m = \boldsymbol{r}_i + \boldsymbol{R}_m - \boldsymbol{r}_j$ . On the other hand, the integral of the matrix element $\Theta_{ij}(\boldsymbol{k})$ for the constant term (when $\hat{\varepsilon}_c^{-1} = \hat{1}$) is

$$\Theta_{ij}^{\mathrm{empty}}(\boldsymbol{k}) = \sum_m \frac{\pi\alpha^2}{2} \mathrm{e}^{-\mathrm{i}\boldsymbol{k}\cdot\boldsymbol{R}_m} \mathrm{e}^{-\frac{{r'_m}^2}{2\alpha^2}} \frac{1}{\alpha^2} \left(2 - \frac{{r'_m}^2}{\alpha^2}\right). \quad (15)$$

For the empty lattice, all the matrix elements of Eq. (9) are given by using Eqs. (14) and (15). When some structures are introduced, the additional work to obtain matrix elements is the numerical integration within the structures.

### B. Gaussian basis set (3D case)

For a 3D system, it is generally impossible to decompose the EM fields into TE or TM modes, and we have to handle all three components of the vector eigenequation. A naive thought suggests us to use the scalar Gaussian functions [Eq. (13)] for each component of the vector as

$$\boldsymbol{\psi}_k(\boldsymbol{r}) = \sum_{\lambda=1}^{3} \boldsymbol{e}_\lambda \sum_i c_{ik}^\lambda g_{ik}(\boldsymbol{r}). \quad (16)$$

Here, $\boldsymbol{e}_\lambda$ represents unit vectors in three orthogonal directions. This naively introduced basis set, however, has a deficiency in the following sense. Firstly, note that the divergence of the Eq. (3) vanishes because of $\nabla \cdot (\nabla \times \boldsymbol{f}(\boldsymbol{r})) = 0$ for any vector field $\boldsymbol{f}(\boldsymbol{r})$. Thus, when the permeability is constant and isotropic, the solution of Eq. (3) satisfies the constraint,

$$\nabla \cdot \boldsymbol{H}(\boldsymbol{r}) = 0. \quad (17)$$

On the other hand, the divergence of Eq. (16) is

$$\nabla \cdot \sum_{i,\lambda} \boldsymbol{e}_\lambda c_{ik}^\lambda g_{ik}(\boldsymbol{r}) = \sum_{i,\lambda} \left(-2\alpha x_\lambda\right) c_{ik}^\lambda g_{ik}(\boldsymbol{r}) \,, \tag{18}$$

where the right-hand side does not vanish except in the trivial case with $c_{ik}^\lambda = 0$ for all combinations of $i$ and $\lambda$. Namely, expansion Eq. (16) does not satisfy constraint Eq.(17), and as a consequence, the spectrum of the eigenvalues includes unphysical spurious values. For each basis to satisfy constraint Eq. (17), we modify each basis by taking its rotation as

$$\begin{aligned} \boldsymbol{g}_{ik}^\lambda(\boldsymbol{r}) &= \nabla \times \boldsymbol{e}_\lambda g_{ik}(\boldsymbol{r}) \\ &= \sum_{\mu,\nu=1}^{3} \varepsilon_{\mu\lambda\nu} \left(-2\alpha x_\mu\right) g_{ik}(\boldsymbol{r})\, \boldsymbol{e}_\nu, \end{aligned} \tag{19}$$

where $\varepsilon_{\lambda\mu\nu}$ is an anti-symmetric symbol ($\varepsilon_{123} = 1$). This is also obtained by choosing three independent basis elements of the lowest order from Eq. (7) under the divergence-free condition. The modified basis element Eq. (19) has no divergence, and satisfies the constraint [Eq. (17)]. We expand the solution using these basis elements as

$$\boldsymbol{\psi}_k(\boldsymbol{r}) = \sum_{\lambda=1}^{3} \sum_i c_{ik}^\lambda \boldsymbol{g}_{ik}^\lambda(\boldsymbol{r}) \,. \tag{20}$$

Here again, we write down the integral values for this basis set. The integrals for the constant term of the overlaps $O_{iz,jz}\left(\boldsymbol{k}\right)$ and $O_{ix,jz}\left(\boldsymbol{k}\right)$ are

$$\begin{aligned} O_{iz,jz}^{\mathrm{empty}}(\boldsymbol{k}) = \sum_m \sqrt{\left(\frac{\pi\alpha^2}{2}\right)^3} \mathrm{e}^{-\mathrm{i}\boldsymbol{k}\cdot\boldsymbol{R}_m} \mathrm{e}^{-\frac{{r'_m}^2}{2\alpha^2}} \\ \times \frac{1}{\alpha^2}\left\{2 - \frac{1}{\alpha^2}\left({x'_m}^2 + {y'_m}^2\right)\right\} \end{aligned} \tag{21}$$

$$O_{ix,jz}^{\mathrm{empty}}(\boldsymbol{k}) = \sum_m \sqrt{\left(\frac{\pi\alpha^2}{2}\right)^3} \mathrm{e}^{-\mathrm{i}\boldsymbol{k}\cdot\boldsymbol{R}_m} \mathrm{e}^{-\frac{{r'_m}^2}{2\alpha^2}} \frac{1}{\alpha^4} x'_m z'_m \tag{22}$$

respectively, while the integrals for the matrix elements $\Theta_{iz,jz}\left(\boldsymbol{k}\right)$ and $\Theta_{ix,jz}\left(\boldsymbol{k}\right)$ are

$$\begin{aligned} \Theta_{iz,jz}^{\mathrm{empty}}(\boldsymbol{k}) = \sum_m \sqrt{\left(\frac{\pi\alpha^2}{2}\right)^3} \mathrm{e}^{-\mathrm{i}\boldsymbol{k}\cdot\boldsymbol{R}_m} \mathrm{e}^{-\frac{{r'_m}^2}{2\alpha^2}} \\ \times \frac{1}{\alpha^4}\Big[\frac{1}{\alpha^4}\left({x'_m}^2 + {y'_m}^2\right)^2 - \frac{9}{\alpha^2}\left({x'_m}^2 + {y'_m}^2\right) \\ + \frac{{z'_m}^2}{\alpha^2}\Big\{\frac{1}{\alpha^2}\left({x'_m}^2 + {y'_m}^2\right) - 2\Big\} + 10\Big] \end{aligned} \tag{23}$$

$$\begin{aligned} \Theta_{ix,jz}^{\mathrm{empty}}(\boldsymbol{k}) = \sum_m \sqrt{\left(\frac{\pi\alpha^2}{2}\right)^3} \mathrm{e}^{-\mathrm{i}\boldsymbol{k}\cdot\boldsymbol{R}_m} \mathrm{e}^{-\frac{{r'_m}^2}{2\alpha^2}} \\ \times \frac{x'_m z'_m}{\alpha^6}\left(7 - \frac{{r'_m}^2}{\alpha^2}\right) \end{aligned} \tag{24}$$

respectively. The integrals of the other components are obtained by permutations of the indices $x$, $y$, and $z$. In addition, the integrals are invariant against the simultaneous exchange of the position of the localization center and the direction of the polarization ($i\lambda' \leftrightarrow j\lambda$). Thus all matrix components for an isotropic bulk dielectric are given by Eqs. (22)-(24). The grid points for these basis elements can be chosen to divide the unit cell of the Bravais lattice with a regular spacing like Fig. 1.

Here, we make some comments on the case of spatially varying $\hat{\mu}(\boldsymbol{r})$. In such a case, we have $\nabla \cdot \boldsymbol{H}(\boldsymbol{r}) \neq 0$, but the expansion (Eq. (16)) still produces a spurious spectrum. However, the basis set (Eq. (19)) is also insufficient because it has no longitudinal component of $\boldsymbol{H}(\boldsymbol{r})$, which should arise in this case.

### C. Chern number calculation

The most sophisticated method for the calculation of the Chern number seems to be the one devised by Fukui, Hatsugai and Suzuki[40]. Here, let us review the method briefly. In this method, the Chern number is derived on a discretized mesh of the Brillouin zone. An $U(1)$ link variable is defined as

$$U_\mu(\boldsymbol{k}_l) \equiv \frac{\langle n(\boldsymbol{k}_l) \left| n(\boldsymbol{k}_l + \mathbf{e}_\mu)\right\rangle}{\left|\langle n(\boldsymbol{k}_l) \left| n(\boldsymbol{k}_l + \mathbf{e}_\mu)\right\rangle\right|}, \tag{25}$$

where $|n(\boldsymbol{k}_l)\rangle$ is the $n$th eigenvector obtained by diagonalizing an eigenequation, $\boldsymbol{k}_l$ represents a lattice point in the discretized, Brillouin zone and $\mathbf{e}_\mu$ represents one lattice displacement in the direction $\mu\,(=1,2)$. The $\boldsymbol{k}_l$ is invariant under the displacement of periodic length $\boldsymbol{k}_l + N_\mu \mathbf{e}_\mu = \boldsymbol{k}_l$. From the link variable, a lattice field strength is taken as

$$\begin{aligned} \tilde{F}_{12}(\boldsymbol{k}_l) \equiv \ln U_1(\boldsymbol{k}_l)\, U_2(\boldsymbol{k}_l + \mathbf{e}_1)\, U_1^{-1}(\boldsymbol{k}_l + \mathbf{e}_2)\, U_2^{-1}(\boldsymbol{k}_l) \\ -\pi < \frac{1}{\mathrm{i}} \tilde{F}_{12}(\boldsymbol{k}_l) \leq \pi. \end{aligned} \tag{26}$$

Here the field strength is defined as the principal branch of the logarithm. From this field strength, the Chern number is computed as

$$\tilde{c} = \frac{1}{2\pi\mathrm{i}} \sum_l \tilde{F}_{12}(\boldsymbol{k}_l) \,, \tag{27}$$

where the sum is taken over all the lattice points in Brillouin zone. It is straightforward to extend this method to multiband cases.

Equation (26) naturally reflects gauge invariance. The result is always given as an integer because of the periodicity of the parameters ($|n(\boldsymbol{k}_l + N_\mu \mathbf{e}_\mu)\rangle = |n(\boldsymbol{k}_l)\rangle$) and it can be seen by fixing the gauge over the entire lattice points. A gauge potential is defined as

$$\widetilde{A}_\mu(\boldsymbol{k}_l) = \ln U_\mu(\boldsymbol{k}_l) \,, \quad -\pi < \frac{1}{\mathrm{i}} \widetilde{A}_\mu(\boldsymbol{k}_l) \leq \pi, \tag{28}$$

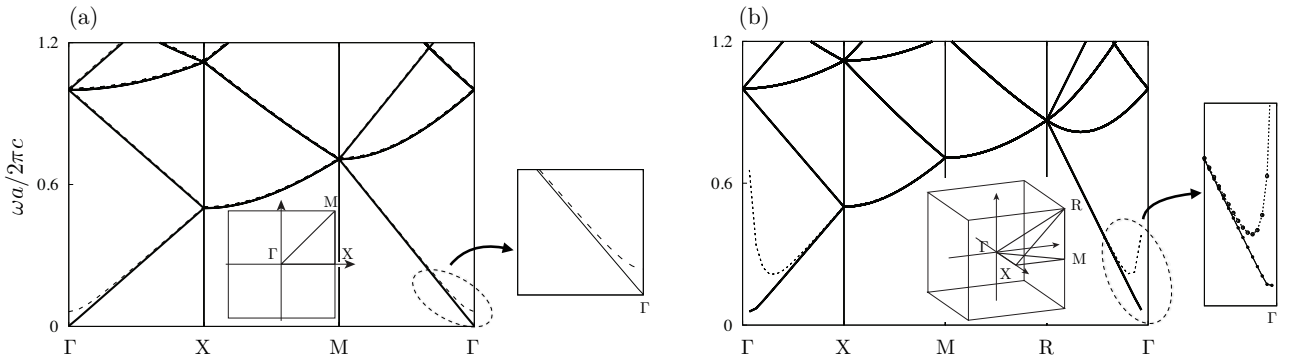


FIG. 2. Band structures of empty lattices (homogeneous systems $\hat{\varepsilon} = \hat{1}$ and $\hat{\mu} = \hat{1}$). (a) Dispersion of 2D square empty lattice calculated by using 64 ($8 \times 8$) scalar Gaussian basis elements. The basis elements are located on grid points that regularly the divide square lattice. Results of different settings are compared between $\alpha = d$ (solid lines) and $\alpha = 0.83d$ (broken lines). For the basis set with smaller overlap (broken line),the lowest eigenvalue at Γ point does not converge to 0. (b) Dispersion of 3D simple cubic empty lattice calculated by using 1,536 basis elements with $\alpha = 1.07d$ (solid lines) and $\alpha = d$ (broken line). The fictitious divergence of the lowest eigenvalue near Γ suppressed by taking larger overlap (solid line). The lowest eigenstate at Γ point cannot be restored by the vector Gaussian basis set.

which is periodic on the lattice $\tilde{A}_\mu(\boldsymbol{k}_l + N_\mu \mathbf{e}_\mu) = \tilde{A}_\mu(\boldsymbol{k}_l)$. The field strength (Eq. (26)) is related to this gauge potential by

$$\tilde{F}_{12}(\boldsymbol{k}_l) = \triangle_1 \widetilde{A}_2 - \triangle_2 \widetilde{A}_1 + 2\pi \mathrm{i} n_{12}(\boldsymbol{k}_l)\,, \qquad (29)$$

where $\triangle_\mu$ represents a forward difference operation $\triangle_\mu \widetilde{\boldsymbol{A}}(\boldsymbol{k}_l) = \widetilde{\boldsymbol{A}}(\boldsymbol{k}_l + \boldsymbol{e}_\mu) - \widetilde{\boldsymbol{A}}(\boldsymbol{k}_l)$ and $n_{12}(\boldsymbol{k}_l)$ is an integer-valued field that makes $-\pi < \tilde{F}_{12}/\mathrm{i} \leq \pi$. Taking the sum of Eq. (29), the first and second terms of the right hand side cancel between adjacent links. Then the total sum of those terms vanishes because of the periodicity, and the result is given by

$$\tilde{c} = \sum_l n_{12}(\boldsymbol{k}_l)\,. \qquad (30)$$

For the Gaussian(spatially localized) basis sets, $|n(\boldsymbol{k})\rangle$ is given by the eigenvector of the matrix eigenequation (Eq. (9)). Since Eq. (9) is invariant under the displacement $\boldsymbol{k} \to \boldsymbol{k} + \boldsymbol{G}$, it is guaranteed that the computed Chern number is an integer.

## III. TEST FOR THE METHOD

### A. Empty lattice

In this subsection, we give appropriate settings for the Gaussian basis sets to produce sufficiently accurate results for empty lattices in 2D and 3D cases. Further, using the determined setting, we calculate band structures of typical photonic crystals of both 2D and 3D as examples.

Let us begin with the 2D empty lattice, in which the equation to be solved becomes a scalar equation. The results for a square lattice are shown in Fig. 2(a) for two different settings represented as solid and broken lines. For both of the settings, we use 64 basis elements on regularly aligned grid points, i.e., eight basis elements per each direction. The broken line is obtained by setting the localization factor in the $\mathrm{e}^{-r^2/\alpha^2}$ to $\alpha = 0.87d$ ($d$ being the spacing between two gird points) and the solid line is obtained by setting it to $\alpha = d$. A good convergence for these settings requires matrix elements up to the fifth-nearest-neighbor pairs of the grid points. The necessary furthest pairs for matrix elements are determined by the overlap length of the matrix $\Theta$ since the convergence of the matrix elements of $\Theta$ is slower than those of $O$.

Within the shown frequency scale, the solid and broken lines overlap well and the solid lines match perfectly with the analytically derived dispersion, namely, $\omega = ck$ folded in the first Brillouin zone. However, at the Γ-point, the lowest band does not converge to $\omega \to 0$, in $k \to 0$ limit. This mismatch comes from the fact that the Gaussian basis elements should have sufficiently large overlaps between them in order to compose a spatially homogeneous state, which is expected to be realized in the $\omega \to 0$ and $k \to 0$ limit. On the other hand, the accuracy for higher frequency modes is improved by increasing the number of basis elements since higher modes vary more rapidly in space. The failure in the $\omega \to 0$ limit is usually irrelevant in the discussion of topological states, since we usually focus on photonic gaps at finite $\omega$ to see topological phenomena.

For the 3D case, the vector equations should be treated and the basis set $\left\{ |\tilde{\boldsymbol{g}}^\lambda_{ik}\rangle \right\}$ is used. Also in this case, the exact band structure of the empty lattice is well restored by using $1,536$ basis elements, i.e., 512 grid points with eight grid points per each direction, and three basis elements ($\lambda = 1, 2, 3$) on each grid point. The results are

shown in Fig. 2(b) for two different settings. The broken line is obtained by setting the localization factor in the $|\tilde{\boldsymbol{g}}^{\lambda}_{ik}\rangle$[Eq. (19)] to $\alpha = d$ and the solid line is obtained by setting it to $\alpha = 1.07d$. However, since the $|\tilde{\boldsymbol{g}}^{\lambda}_{ik}\rangle$ is the Gaussian function multiplied by the first-order polynomial, it extends in a broader region than the genuine Gaussian function does.

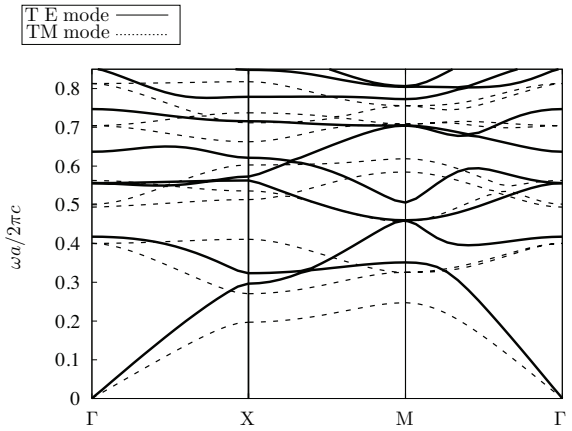


FIG. 3. Calculated band structure of dielectric columns arranged in a square lattice in air with radius $r = 0.378a$. We set the relative permittivity $\varepsilon = 8.9$ in columns ($\varepsilon = 1$ in air). Solid lines (dashed lines) represents TE (TM) mode dispersion. The calculation is performed using 64 basis elements with $\alpha = d$.

The difference of the first eigenvalues between $\alpha = d$ and $\alpha = 1.07d$ near Γ-point is more prominent than the 2D case. We have confirmed that the results are well converged and match perfectly to the dispersion, $\omega = ck$, folded in the first Brillouin zone in the shown frequency scale when we set $\alpha$ more than $1.07d$, which takes the matrix elements up to the 8th nearest neighbor points. Yet the lowest eigenmode at Γ point is never restored with the basis set $\{|\tilde{\boldsymbol{g}}^{\lambda}_{ik}\rangle\}$, due to the difficulty in representing a uniform field by $|\tilde{\boldsymbol{g}}^{\lambda}_{ik}\rangle$, since $|\tilde{\boldsymbol{g}}^{\lambda}_{ij}\rangle$ is an odd function with respect to its center.

### B. The case of spatially modulated permittivity

To begin with, we choose an array of dielectric columns arranged on a square lattice as a sample system for the 2D Gaussian basis set. We assume the radius of the column to be $0.378a$ with $a$ representing the lattice spacing, and the relative permittivity to be $\varepsilon = 8.9$ within the columns ($\varepsilon = 1.0$ out of the columns)[24]. The calculated dispersions for TE modes (solid lines) and TM modes (dashed lines) are shown in Fig. 3. The calculation is done with the same setting as the empty lattice [the solid line in Fig. 2(a)]. The numerical integration between Gaussian basis elements converges by fining the integral mesh up to $\alpha/5$. The precision of the results increases with the number of basis elements in one direction $n_x$. In this system, the most of eigenvalues converge in the shown scale before $n_x = 8$, with which the result in Fig. 3 is obtained.

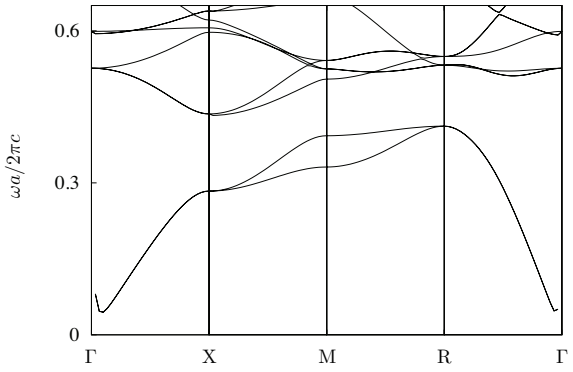


FIG. 4. Calculated band structure of the three-dimensional square rod structure with the width of rod being $0.26a$ and the relative permittivity $\varepsilon = 13.0$. The calculation is performed using 1,536 basis elements with $\alpha = 1.07d$.

In this case, the radius of the column $r = 0.378a$ is relatively large compared to the size of the unit cell. Therefore the structure is smooth and well restored with the integral mesh $\alpha/5$ for $n_x = 8$. However, when the radius of the column is smaller, the basis set has to detect a finer structure in integration and we need a larger number of basis elements, which implies slower convergence. Another potential source of bad convergence is a sharp structure such as a corner of a rectangular rod, and we should be careful when such a structure is treated in the present method.

Next, we choose a simple scaffold structure, namely a three-dimensional square rod structure studied by Sözüer and Haus[37], as an example system for the 3D Gaussian basis set. We assume the width of the rod as $0.26a$ and the relative permittivity $\varepsilon = 13.0$, which is the same situation as in the study of Dobson *et al.*[25]. The result shown in Fig. 4 is obtained with the same setting as in the empty lattice case [the solid line in Fig. 2(b)]. As known, there exists full gap between the fifth and sixth bands. As in the case of the empty lattice, there is difficulty in the $\omega \to 0$ and $k \to 0$ limit, however, except that point, the global profile of the calculated band structure, such as the existence of the full gap, is consistent with that of the previous works.

## IV. SECTION CHERN NUMBERS AND EDGE STATES IN A 3D PHOTONIC CRYSTAL

In this section, we demonstrate the topologically protected edge states of EM waves associated with the finite section Chern number in a 3D photonic crystal with broken SIS.

In a 3D periodic system, the wave vector has three components, $k_1$, $k_2$, and $k_3$, and the section Chern number is defined using two of them, regarding the remaining one as a free parameter. If we fix $k_3$, the section Chern number $C_n(k_3)$ is defined as

$$\begin{aligned} C_n(k_3) &= \frac{1}{2\pi \mathrm{i}} \int \mathrm{d}k_1 \mathrm{d}k_2 \; B_{n,12}(\boldsymbol{k}), \\ B_{n,12}(\boldsymbol{k}) &= \partial_{k_1} \mathcal{A}_{n,2}(\boldsymbol{k}) - \partial_{k_2} \mathcal{A}_{n,1}(\boldsymbol{k}), \\ \mathcal{A}_{n,i}(\boldsymbol{k}) &= \langle \psi_n(\boldsymbol{k}) | \partial_{k_i} | \psi_n(\boldsymbol{k}) \rangle, \end{aligned} \tag{31}$$

and those defined by fixing $k_1$ or $k_2$ are similarly given by permutations of the components $(k_1, k_2, k_3) \to (k_2, k_3, k_1) \to (k_3, k_1, k_2)$. In order to make $C_n(k_3)$ well-defined, the gap should remain finite over the entire $k_3$ constant plane. In general, the section Chern number takes any value, but the symmetry of a given system induces restriction. If a system has TRS, the eigenstate for $\boldsymbol{k}$ is related to that for $-\boldsymbol{k}$ by the bosonic time-reversal operation $\mathcal{T}$, as $\mathcal{T}|\psi_n(\boldsymbol{k})\rangle = |\psi_n(-\boldsymbol{k})\rangle^*$, which leads to $\boldsymbol{B}_n(-\boldsymbol{k}) = -\boldsymbol{B}_n(\boldsymbol{k})$. Then, we have $C_n(k_3) = 0$ for $k_3 = 0$ and $\pi$, because of $B_n(-k_1, -k_2, 0) = -B_n(k_1, k_2, 0)$ and $B_n(-k_1, -k_2, -\pi(=\pi)) = -B_n(k_1, k_2, \pi)$, and the definition Eq. (31). If there is SIS in addition to TRS, an additional restriction may arise, that is, SIS gives $|\psi_n(-\boldsymbol{k})\rangle = |\psi_n(\boldsymbol{k})\rangle$, which indicates $\boldsymbol{B}_n(-\boldsymbol{k}) = \boldsymbol{B}_n(\boldsymbol{k})$, and if this relation is combined with $\boldsymbol{B}_n(-\boldsymbol{k}) = -\boldsymbol{B}_n(\boldsymbol{k})$ required by TRS, we finally obtain $\boldsymbol{B}_n(\boldsymbol{k}) = -\boldsymbol{B}_n(\boldsymbol{k}) = 0$. Therefore, SIS has to be broken for a nonzero section Chern number if the system has TRS.

Owing to the topological nature of $C_n(k_3)$, when $C_n(k_3)$ changes as a function of $k_3$, there should be a gap closing point somewhere on the corresponding $k_3$ constant plane. On the other hand, as we have noted, the section Chern number is always zero at $k_3 = 0$ and $\pi$ with TRS. These facts indicate that the finite section Chern number requires existence of a gap closing point. Typically, gap closing occurs on isolated points in the Brillouin zone and the linear dispersion appears around those degeneracy points. A degeneracy point with linear dispersion is named as a Weyl point. Note that $k_z$ appearing in the section Chern number $C_n(k_z)$ is related to the fixed $k_z$ of an incident wave on the photonic crystal.

### A. Honeycomb array of air hole columns

Now, we consider to realize Weyl points in photonic crystals. In specific, we need a system in which the Weyl point related physics is readily accessible. More specifically, in order to observe chiral edge modes associated with the finite section Chern number $C_n(k_3)$, it is required to have a clear gap on the entire two-dimensional plane with fixed $k_3$. Since a clear gap is required only on a fixed $k_3$ plane, a possible strategy to achieve our goal is to start with a two-dimensional system having "pseudo-gap," a frequency region filled with only a few bands, and then to apply appropriate three-dimensional modifications to the system. Because we are handling photonic crystals, the band structure can be modified by controlling the background medium. However, our experience tells us that careless modifications prone to fail, namely, even if Weyl points are successively generated, they are often masked by the other dispersive bands. Hence, the careful design is important and this is what we discuss in the following.

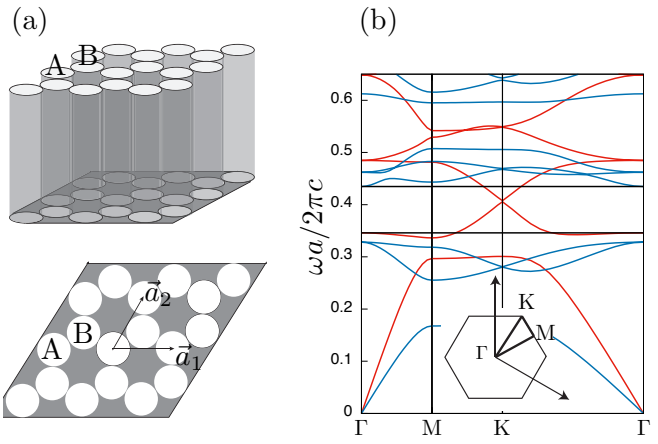


FIG. 5. (Color online) (a) Honeycomb array of hollow columns in a dielectric material. (b) Two-dimensional dispersion of the photonic crystal. We use permittivity $\varepsilon = 20.0$, the radius of hollow column $r = \sqrt{3}a/6$. The band structure of TE modes (red line) has a distinctive degeneracy point, which is clear (indicated by black lines) in the $k_z = 0$ plane among both of TE and TM modes.

In order to realize easily accessible Weyl points, we consider a photonic crystal of hollow columns aligned on the honeycomb lattice as depicted in Fig. 5. The band structure of this system has some similarity to that of the triangular lattice consisting of dielectric columns[36]. This is because the complementary region of the hollow honeycomb lattice composes a triangular lattice. Despite this similarity, we choose to use the hollow honeycomb lattice since it turns out that the existence of the sublattice structure of the honeycomb lattice is advantageous in the following discussion. Without three-dimensional modulation, the second and third TE modes of the hollow honeycomb lattice form 2D Dirac cones at K and K' points, and TM modes do not mask these TE Dirac cones.

Owing to SIS of the hollow honeycomb lattice, these TE Dirac cones are actually line degeneracies extending in the $k_z$ direction in the three-dimensional Brillouin zone. Then, SIS should be broken to transform the line

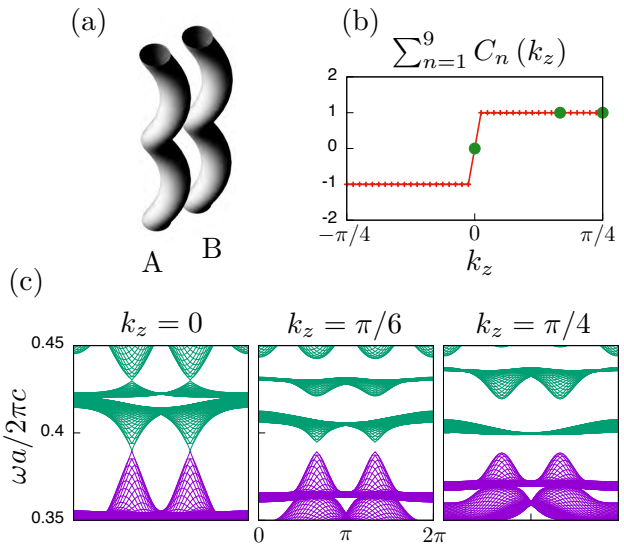


FIG. 6. (Color online) (a) Columns are modulated into helices with the same twists for sublattices A and B. The radius of the twisting circle is taken to be $r_h = 0.05a$ and it circles one time with translation in the $z$ direction by a unit length $a$. The system does not have SIS but is invariant under the twofold rotation around the $z$ axis and the axis perpendicular to the $z$ axis. (b) The value of the total section Chern number summed up to the 9th band for each $k_z$ ($-\pi/4 \leq k_z \leq \pi/4$). (c) Bulk band dispersions for several values of $k_z$. The 1-9th bands are represented by purple lines.

degeneracy into Weyl points, and therefore, we reshape each hollow column into a hollow helix. Note that it is possible to modulate columns differently on sublattices A and B of the honeycomb lattice.

### B. Weyl points and change in section Chern number

Now, we consider to apply the same twist on the both hollows at sublattices A and B (Fig. 6). By transforming columns into helices, the SIS is broken and the line degeneracy is lifted except K and K' points, which implies emergence of the Weyl points. This emergence is explained in terms of the point group symmetry as follows. Before the twist is applied, the system has $D_{6h}$ symmetry, and the group of $k$ is $C_{3v}$ on the line parallel to the $k_z$ axis passing through K and K' points, whereas it is $D_{3h}$ for K and K' points. Since both of $C_{3v}$ and $D_{3h}$ contain two-dimensional representations, twofold degeneracy is allowed on the whole line, which supports existence of the line degeneracy without twist. Then, after applying the twist, the reflection symmetry with respect to a plane including the $z$ axis is broken and the group of $k$ on the line parallel to the $k_z$ axis passing through K and K' points turns to $C_3$, except K and K' points. This implies the line degeneracy dissolves except K and K' points since $C_3$ has no multidimensional representation. For K and K' points, the group of $k$ changes from $D_{3h}$ to $D_3$. By the compatibility relation, 2D representations of $D_{3h}$ are connected to 2D representations of $D_3$, and therefore, the degeneracies at K and K' points survive even with the twist.

The surviving degeneracy points are two Weyl points with the same chirality since these points are related by two-fold rotation around the $z$ axis. Then, the section Chern number $C_n(k_z)$ changes by $\pm 2$ when $k_z$ crosses $k_z = 0$, because of *two* Weyl points on the $k_z = 0$ plane [Figs. 6(b) and 6(c)]. The exactly same argument also applies for the $k_z = \pi$ plane, but it is not possible to resolve Weyl points on the $k_z = \pi$ plane, since the bands on which we focus merge into the other bands as we increase $k_z$ from 0 to $\pi$. Note that the observation of $\pm 2$ jump in $C_n(k_z)$ at $k_z = 0$ does not contradict with the former statement that $C_n(0)$ should be 0, since at that time we had assumed that the gap is finite on entire $k_z = 0$ plane, and this assumption is invalid in this case.

Next, we consider to change the twist of helix only for the hollow on the sublattice B [Fig. 7(a)]. With this modification, the twofold rotational symmetry around the $k_z$ axis and the axis perpendicular to $k_z$ axis are broken and then, there is no reason to have degeneracy on the $k_z = 0$ plane. However, the Weyl points found in Fig. 6(c) do not simply disappear because Weyl points are topologically stable and only disappear by annihilating as a pair of Weyl points with opposite chiralities[47]. Our numerical calculation shows that the Weyl points move to $\pm k_z$ directions as we increase the difference of the radius of the helices. When one of the Weyl points moves in $+k_z$ direction, the other one moves in $-k_z$ direction due to TRS. In this case, the dispersion is fully gapped on the $k_z = 0$ plane, and we have $C_n(0) = 0$, which is consistent with the former statement. The section Chern number becomes finite for large enough $k_z$ as expected from the existence of the Weyl points.

### C. Edge modes

In order to investigate edge modes, we perform calculations using the developed Gaussian basis elements on the photonic crystal truncated in the $\vec{a}_1$ direction [see Fig. 8(b) for the definition of $\vec{a}_1$] with finite width (eight unit cells in specific). At the interface, we place a material with a smaller dielectric constant so as to prevent the light from evading to outside. This is necessary because the momentum/frequency region we are focusing on lies above the light cone (for the same dielectric constant with the hollow region), which means that the light is able to escape from the system.

In Figs. 8 and 9, the dispersion relations of the finite width system are compared with the bulk dispersions projected on the surface for several values of $k_z$. We find several bands apart from the bulk contribution, which signals the existence of edge modes. In fact, it is

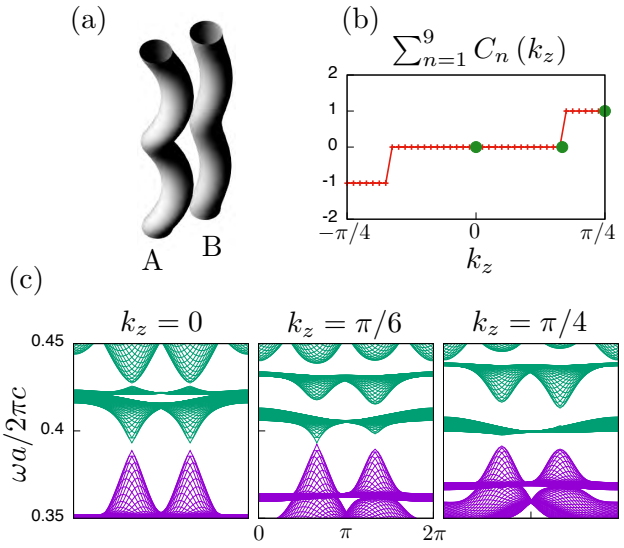


FIG. 7. (Color online) (a) Different twists for sublattices A and B, with the twisting circle for helix A being $r_{h,A} = 0.05a$ and for helix B being $r_{h,B} = 0.03a$. (b) The value of the total section Chern number summed up to the ninth band for each $k_z$ ($-\pi/4 \leq k_z \leq \pi/4$). (c) Bulk band dispersions for several values of $k_z$. The first to ninth bands are represented by purple lines.

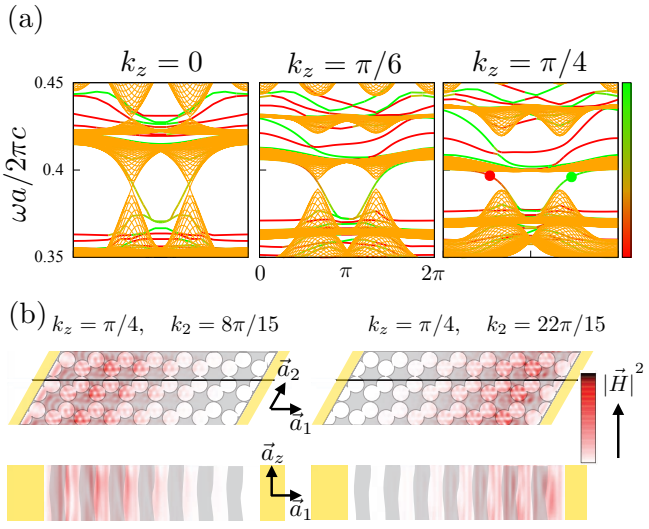


FIG. 8. (Color online) (a) The dispersion curve (color spectrum) for a finite width system (eight unit cells) that corresponds to Fig. 6 in bulk, plotted with projected bulk dispersion (yellow lines). The color spectrum indicates on which side the eigenstate inclines by red (left) - yellow (middle) - green (right). (b) The profile of the $n$th eigenstate for $k_z = \pi/4$, $k_2 = (4/15)2\pi$ and $k_2 = (11/15)2\pi$, which are indicated by the points in the right most panel of (a).

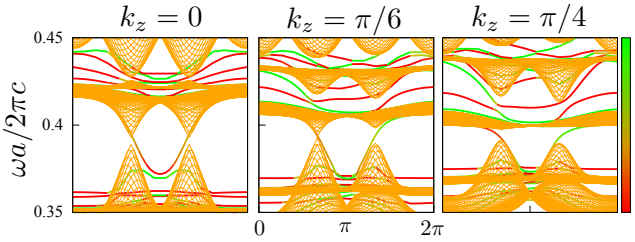


FIG. 9. (Color online) The dispersion curve (with color spectrum) for a finite width system (eight unit cells) that corresponds to Fig. 7 in bulk, plotted with projected bulk dispersion (yellow lines). See the caption of Fig. 8 for the description of the color spectrum.

confirmed that the non-bulk bands are localized at the interfaces by examining the eigenvector for each mode. The eigenvectors also tell us on which side, left or right, each mode localizes. In Figs. 8 and 9, the red color corresponds to the states on the left edge, while the green color to the states on the right edge. The color spectrum is determined by the moment of the eigenfield $\langle r_1 \rangle_{\boldsymbol{H}_{n,k}} = \int \mathrm{d}^3 r \; r_1 \vec{H}^2_{n,k}(\boldsymbol{r})$. As we change $k_z$, the way that the edge modes connect bulk bands changes in accordance with the change of the sum $\sum_{n=1}^{9} C_n(k_z)$, which confirms the bulk-edge correspondence. The same argument also applies to gaps other than the 9th gap with nonzero total section Chern number. When the fixed momentum is conserved for $k_z$ with $\sum_{n=1}^{i} C_n(k_z)$ being nonzero, the wave propagates unidirectionally along the interface.

This photonic crystal has the structure similar to the honeycomb array of twisted waveguides studied by Rechtsman *et al.*[17], where evanescently coupled modes are considered. In the system of evanescently coupled waveguides, the $z$ axis, which is the propagation direction of a waveguide mode, is regarded as the *temporal* axis and the system is spatially two-dimensional. There, the twist of a waveguide becomes a temporal periodic modulation for waveguide modes and the appearance of the chiral edge modes is attributed to the Chern number for the *Floquet* band structure. On the other hand, we consider, in this paper, TE-like modes in the spatially three-dimensional photonic crystal and relate the unidirectional propagation of them to the finite value of section Chern numbers.

Depending on the dielectric constant of the material, there might exist some wave guide modes near the frequency of the Weyl point and it leads to coupling between edge modes and wave guide modes that extend into bulk. In such a case, it is possible to suppress the mixing between the edge modes and the wave guide modes by shifting the relative positions of them in the frequency space. The relative shift can be achieved by changing the pitch of the helix while keeping its twist unchanged because the dispersion of wave guide modes is easily affected by

the periodic length in the $z$ direction, whereas that of TE-like modes is not affected so much.

## V. SUMMARY

We proposed the Gaussian basis sets for the calculation of EM fields in 2D and 3D photonic crystals. In the formulation with spatially localized basis elements, the wave number appears as a boundary condition in the eigenequation and the eigenequation strictly becomes periodic in the wave number, which is advantageous for the Chern number calculation. In addition, the localized property of the Gaussian basis element becomes effective for the consideration of finite size or interface effects, which usually requires larger systems, by utilizing iterative algorithms. Besides, in three-dimensional cases, the Gaussian basis element can easily be accommodated to the divergence-free constraint of the Maxwell equations due to its simplicity for differentiation operation. For further improvement, it would be expected to optimize the mesh alignment or the localization factor of the Gaussian basis elements for each structure.

We demonstrated the bulk-edge relation between the section Chern number and chiral edge modes in the SIS broken 3D photonic crystal with TRS. It was confirmed that chiral edge modes in the $n$th gap at each $k_z$ reflects the total of the section Chern number below the $n$th gap $C_n(k_z)$. A system with a finite section Chern number is expected to lead to some applications for wave-packet dynamics. For simplicity, we take a situation that the Weyl points exist on the $k_z = 0$ plane. When a wave packet is injected into the finite width system of the SIS broken 3D photonic crystal, a wave packet composed of the Bloch states with positive $k_z$ does propagate on the one side, but does not on the other side. If we use the Bloch states with negative $k_z$, the side that allows propagation changes. In this way, the system is useful to filter wave packets with fixed sign of $k_z$.

## ACKNOWLEDGMENTS

We thank S. Takahashi and S. Iwamoto for fruitful discussions. This work is partly supported by Grants-in-Aid for Scientific Research, Nos. 26247064, 25107005, and 16K13845 from JSPS. The computation in this work has been done using the facilities of the Supercomputer Center, the institute for Solid State Physics, the University of Tokyo.

* oono@rhodia.ph.tsukuba.ac.jp

[1] E. Yablonovitch, Phys. Rev. Lett. **58**, 2059 (1987).
[2] J. D. Joannopoulos, S. G. Johnson, J. N. Winn, and R. D. Meade, *Photonic Crystals: Molding the Flow of Light* (Princeton University Press, Princeton, 2008).
[3] K. Sakoda, *Optical Properties of Photonic Crystals* (Springer, Berlin, 2004).
[4] K. v. Klitzing, G. Dorda, and M. Pepper, Phys. Rev. Lett. **45**, 494 (1980).
[5] D. J. Thouless, M. Kohmoto, M. P. Nightingale, and M. den Nijs, Phys. Rev. Lett. **49**, 405 (1982).
[6] R. B. Laughlin, Phys. Rev. B **23**, 5632 (1981).
[7] Y. Hatsugai, Phys. Rev. B **48**, 11851 (1993).
[8] Y. Hatsugai, Phys. Rev. Lett. **71**, 3697 (1993).
[9] S. Raghu and F. D. M. Haldane, Phys. Rev. A **78**, 033834 (2008).
[10] Z. Wang, Y. D. Chong, J. D. Joannopoulos, and M. Soljačić, Phys. Rev. Lett. **100**, 013905 (2008).
[11] Z. Wang, Y. Chong, J. D. Joannopoulos, and M. Soljacic, Nature **461**, 772 (2009).
[12] T. Ochiai and M. Onoda, Phys. Rev. B **80**, 155103 (2009).
[13] M. Hafezi, E. A. Demler, M. D. Lukin, and J. M. Taylor, Nat Phys **7**, 907 (2011).
[14] K. Fang, Z. Yu, and S. Fan, Nat Photon **6**, 782 (2012).
[15] M. Hafezi, S. Mittal, J. Fan, A. Migdall, and J. M. Taylor, Nat Photon **7**, 1001 (2013).
[16] A. B. Khanikaev, S. Hossein Mousavi, W.-K. Tse, M. Kargarian, A. H. MacDonald, and G. Shvets, Nat Mater **12**, 233 (2013).
[17] M. C. Rechtsman, J. M. Zeuner, Y. Plotnik, Y. Lumer, D. Podolsky, F. Dreisow, S. Nolte, M. Segev, and A. Szameit, Nature **496**, 196 (2013).
[18] L. Lu, L. Fu, J. D. Joannopoulos, and M. Soljacic, Nat. Photon **7**, 294 (2013).
[19] L. Lu, J. D. Joannopoulos, and M. Soljacic, Nat Photon **8**, 821 (2014).
[20] L. Lu, Z. Wang, D. Ye, L. Ran, L. Fu, J. D. Joannopoulos, and M. Soljai, Science **349**, 622 (2015).
[21] L.-H. Wu and X. Hu, Phys. Rev. Lett. **114**, 223901 (2015).
[22] J.-M. Jin, *The Finite Element Method in Electromagnetics* (Wiley-IEEE Press, Hoboken, 2014).
[23] W. Axmann and P. Kuchment, J. Comp. Phys. **150**, 468 (1999).
[24] D. C. Dobson, J. Comp. Phys. **149**, 363 (1999).
[25] D. C. Dobson, J. Gopalakrishnan, and J. E. Pasciak, J. Comp. Phys. **161**, 668 (2000).
[26] S. Burger, R. Klose, A. Schaedle, F. Schmidt, and L. W. Zschiedrich, in *Integrated Optics: Devices, Materials, and Technologies IX*, edited by Y. Sidorin and C. A. Waechter (SPIE-Intl Soc Optical Eng, Bellingham, 2005).
[27] J. E. Avron, R. Seiler, and B. Simon, Phys. Rev. Lett. **51**, 51 (1983).
[28] B. I. Halperin, Japanese Journal of Applied Physics **26**, 1913 (1987).
[29] M. Kohmoto, B. I. Halperin, and Y.-S. Wu, Phys. Rev. B **45**, 13488 (1992).
[30] Y. Hatsugai, S. Ryu, and M. Kohmoto, Phys. Rev. B **70**, 054502 (2004).
[31] S. Murakami, New Journal of Physics **9**, 356 (2007).
[32] X. Wan, A. M. Turner, A. Vishwanath, and S. Y. Savrasov, Phys. Rev. B **83**, 205101 (2011).
[33] A. A. Burkov and L. Balents, Phys. Rev. Lett. **107**, 127205 (2011).
[34] A. A. Burkov, M. D. Hook, and L. Balents, Phys. Rev. B

**84**, 235126 (2011).
[35] K. M. Ho, C. T. Chan, and C. M. Soukoulis, Phys. Rev. Lett. **65**, 3152 (1990).
[36] M. Plihal and A. A. Maradudin, Phys. Rev. B **44**, 8565 (1991).
[37] H. S. Sözüer and J. W. Haus, J. Opt. Soc. Am. B **10**, 296 (1993).
[38] R. D. Meade, A. M. Rappe, K. D. Brommer, J. D. Joannopoulos, and O. L. Alerhand, Phys. Rev. B **48**, 8434 (1993).
[39] S. G. Johnson and J. D. Joannopoulos, Opt. Express **8**, 173 (2001).
[40] T. Fukui, Y. Hatsugai, and H. Suzuki, J. Phys. Soc. Jpn. **74**, 1674 (2005).
[41] N. Marzari and D. Vanderbilt, Phys. Rev. B **56**, 12847 (1997).
[42] D. M. Whittaker and M. P. Croucher, Phys. Rev. B **67**, 085204 (2003).
[43] K. Busch, S. F. Mingaleev, A. Garcia-Martin, M. Schillinger, and D. Hermann, Journal of Physics: Condensed Matter **15**, R1233 (2003).
[44] N. Marzari, A. A. Mostofi, J. R. Yates, I. Souza, and D. Vanderbilt, Rev. Mod. Phys. **84**, 1419 (2012).
[45] G. Panati, Annales Henri Poincar'e **8**, 995 (2007).
[46] C. Brouder, G. Panati, M. Calandra, C. Mourougane, and N. Marzari, Phys. Rev. Lett. **98**, 046402 (2007).
[47] H. Nielsen and M. Ninomiya, Physics Letters B **130**, 389 (1983).